The circumstellar environments of EP Aqr and Y CVn probed by the H I emission at 21 cm

Thibaut Le Bertre, Éric Gérard

A&A 419, 549–561 (2004)
DOI: 10.1051/0004-6361:20035797

Astronomy & Astrophysics

The circumstellar environments of EP Aqr and Y CVn probed by the H I emission at 21 cm

T. Le Bertre[1] and E. Gérard[2]

[1] LERMA, UMR 8112, Observatoire de Paris, 61 av. de l'Observatoire, 75014 Paris, France
[2] GEPI, UMR 8111, Observatoire de Paris, 5 place J. Janssen, 92195 Meudon Cedex, France

Received 3 December 2003 / Accepted 3 February 2004

Abstract. The H I line at 21 cm has been detected in the circumstellar shells of the two semi-regular variables, EP Aqr and Y CVn, with the Nançay Radio-Telescope (NRT). In both cases the line shape is composite and the emission is spatially extended compared to the NRT beam size (4′). The total H I masses of the two envelopes are respectively ∼0.047 $M_\odot$ and 0.044 $M_\odot$.
For EP Aqr, we find three components: a narrow one centered on the star and spatially unresolved, and two broad, Gaussian components, offset w.r.t. the star and spatially extended. The narrow component traces the present wind from EP Aqr whereas the two others seem to trace one or several mass-loss episodes of long duration.
For Y CVn, we find two components: a narrow, spatially very extended, feature, and a broad one, less extended. We argue that the second component traces the outflow and the first one, its interaction with the ISM.
These observations show that the H I emission can be used not only to probe the mass loss history of long-period variables, but also to investigate the interaction between stellar outflows and the surrounding ISM.

Key words. stars: circumstellar matter – stars: mass-loss – stars: individual: EP Aqr – stars: individual: Y CVn – stars: AGB and post-AGB

1. Introduction

Red giants on the first giant branch (RGB) and on the Asymptotic Giant Branch (AGB) are undergoing mass loss. This phenomenon can occur at any rate, from undetectable ($\leq 10^{-9}$ $M_\odot$ yr^{-1}), to so large ($\sim 10^{-4}$ $M_\odot$ yr^{-1}) that the star may completely disappear at optical and infrared wavelengths. Different phases of mass loss develop on timescales that can take any value from a few years, corresponding to the stellar pulsation period or a multiple of it (Fleischer et al. 1995), to 10^6 years, corresponding to the red giant evolution (e.g. Maeder & Meynet 1988). The common tracers of the mass loss process, mainly dust and CO molecule emissions, react in a complex way to these changes of mass loss rate and to the different timescales. Also, they are representative of only a minute component of the ejected material, whose exact proportion is not well known. Under these conditions, it has been difficult to establish a balance of the mass lost as a function of time, a datum which is seriously needed to describe the post-main sequence evolution of low and intermediate-mass stars ($M \leq 6$–8 $M_\odot$).

Send offprint requests to: T. Le Bertre,
e-mail: Thibaut.LeBertre@obspm.fr

Today the need to use a new tracer of the mass loss phenomenon appears compelling.

The H I line at 21 cm would seem to provide an obvious choice. Hydrogen is expected to be the most abundant element in the material expelled by red giants. Although a part could be locked into molecules like H_2O, most of it should be in atomic form or in the H_2 molecule. Hydrogen is not easily ionized, in the absence of a strong UV field, so that its emission at 21 cm should trace circumstellar shells (CS) on very large scales, at least as compared to the dust whose emission decreases sharply with distance to the central star (due to its dependence on the grain temperature) or to the CO molecule which is photo-dissociated at $\sim 10^{17}$ cm by the interstellar radiation field (ISRF).

This has been recognized by various authors who attempted to detect the H I line at 21 cm in circumstellar envelopes about 20 years ago (e.g. Zuckerman et al. 1980; Bowers & Knapp 1988, BK88). The search was not very fruitful, and only one AGB source, Mira, was clearly detected (BK88). Three main explanations for this situation have been invoked: (i) the emission from H I at 21 cm is weak and difficult to detect; (ii) the interstellar medium along the line of sight often produces an H I emission which makes an intense background against which the circumstellar signal has to be discriminated;

(iii) the hydrogen in the outflows should be molecular rather than atomic. The first two reasons are certainly inescapable, however the third one could be a matter for discussion. Glassgold & Huggins (1983, GH83) argue that the hydrogen flowing out from red giants should be mostly atomic when the central star effective temperature is higher than 2500 K, and molecular in the opposite case. Also Taylor et al. (1990) find H I at 21 cm in absorption against the radio continuum from several planetary nebulae (PN); they ascribe this absorption to the material lost by the central star when it was on the AGB. On the other hand, Gussie et al. (1995) discuss the possibility that H I results from the photodissociation of H_2 by the ISRF and by the central star radiation, an interpretation which is supported by Rodríguez et al. (2002).

The advent of new powerful equipments operating at 21 cm such as the EVLA (Expanded Very Large Array) and SKA (Square Kilometer Array) should revive this field of research. We have taken the opportunity of the recent refurbishment of the Nançay Radio-Telescope (NRT, van Driel et al. 1996) to take a new look at this problem. Our programme aims to detect H I in red giants of the first branch, AGB stars and post-AGBs, including PNs. Our first result has been the detection of H I in the direction of IRC +10216 in absorption against the cosmic background at 21 cm (Le Bertre & Gérard 2001, Paper I). We showed that even if molecular hydrogen might dominate in the internal part of its CS, atomic hydrogen should also be present, at least in the external parts. Then we detected H I from a source with a stellar effective temperature higher than 3000 K, RS Cnc, and argued that the hydrogen in its atmosphere is mostly atomic (Gérard & Le Bertre 2003, Paper II), in contrast with IRC +10216. The implication is that the wind emerging from red giants could be atomic or molecular depending on the stellar effective temperature, as predicted by Glassgold & Huggins (1983). We have presently detected H I in emission in several sources (Gérard & Le Bertre, in preparation), suggesting that atomic hydrogen could be more common than previously thought.

In the present work, we specifically discuss our observations of two long-period variables (LPV), EP Aqr and Y CVn, which illustrate that the H I line profiles contain an unexpected wealth of information on the mass loss from red giants, on the spatial and kinematic structure of CSs and on the interaction between stellar winds and the interstellar medium (ISM).

2. Description of the sources

The two sources have parallaxes measured by Hipparcos, 7.39± 1.19 mas for EP Aqr and 4.59 ± 0.73 mas for Y CVn. Recently Knapp et al. (2003) re-analyzed the Hipparcos data from several LPVs and obtained 3.68 ± 0.83 mas for Y CVn. In the following we adopt distances of 135 pc for EP Aqr and of 218 pc for Y CVn which have already been used by several authors and which facilitate comparisons. The galactic latitudes are −39° for EP Aqr and +72° for Y CVn, which place them at 85 and 207 pc, respectively, from the Galactic Plane.

2.1. EP Aqr

EP Aqr is a semi-regular variable (SRb) of period ∼55 days. Its spectral type is M 8III; Dumm & Schild (1998) evaluate the stellar effective temperature at 3236 K.

The wind from EP Aqr has been studied in the rotational lines of CO. Winters et al. (2003) and Knapp et al. (1998) have produced high-resolution spectra of the CO (1−0), (2−1) and (3−2) lines. All three lines show a composite profile with a narrow component ($V_{\rm exp} \sim 1.4\,{\rm km\,s^{-1}}$) superimposed on a broader one ($V_{\rm exp} \sim 11\,{\rm km\,s^{-1}}$), both centered at $V_{\rm lsr} \sim -34$ km s^{-1}. Kerschbaum & Olofsson (1999) give the same value for the centre velocity ($-33.7\,{\rm km\,s^{-1}}$) of the two CO (1−0) components. However, Olofsson et al. (2002) obtain slightly lower expansion velocities, 1.0 and 9.0 km s^{-1}, through a line-fit accounting for turbulence.

EP Aqr has also been detected in the SiO ($v = 0$, $J = 2$−1) and ($v = 0$, $J = 3$−2) thermal emission by González Delgado et al. (2003). Both lines are centered at $V_{\rm lsr} \sim -32\,{\rm km\,s^{-1}}$ and have a width corresponding to $V_{\rm exp} \sim 8\,{\rm km\,s^{-1}}$. Both lines have spectral profiles with only one component.

The composite CO profile has been interpreted by Knapp et al. as being the result of two successive episodes of mass loss by the central star, an interpretation which is supported by Winters et al. The CO photodissociation radii of these two outflows were estimated to be around 1.1×10^{16} cm (5″) and 2.3×10^{16} cm (11″), respectively.

However, the IRAS data show that the circumstellar envelope is certainly much more extended. Young et al. (1993a) find an extended structure at 60 μm which can be fitted by a detached-shell model with inner radius 1.5′ (or 0.06 pc at 135 pc) and outer radius 5.9′ (or 0.26 pc).

2.2. Y CVn

Y CVn is also a semi-regular variable (SRb), but with a period of 158 days. It is carbon-rich (CGCS 3283; Stephenson 1989) and has a spectral type CIab (C5, 5J). With a $^{12}C/^{13}C$ abundance ratio of 3.5 (Lambert et al. 1986), it belongs to the rare class of J-type stars. Bergeat et al. (2001) estimate its effective temperature at 2760 K, in good agreement with Lambert et al. (1986; 2730 K).

The wind has also been studied in the CO rotational lines. The high-resolution spectra presented by Knapp et al. (1998, 2000) show evidence of only one component with $V_{\rm exp} \sim 9$ km s^{-1}, and centered at $V_{\rm lsr} \sim 21$ km s^{-1}. Neri et al. (1998) have mapped the CO emission and found it to be extended with a size about 13″ in (1−0) and 9″ in (2−1). Noteworthy, Y CVn has been detected in ^{13}CO (1−0) with almost the same intensity as in ^{12}CO (1−0), 5.2 versus 8.3 K km s^{-1}, by Jura et al. (1988). Through a careful modelling, Schöier & Olofsson (2000) derive a circumstellar $^{13}CO/^{12}CO$ abundance ratio of 2.5.

Y CVn has also been detected in the H^{12}CN and H^{13}CN ($J = 1$−0) ground state lines by Izumiura et al. (1987). These emissions are time-variable, probably due to a maser effect, the latter having a peak-intensity of about half the former.

Again the far-infrared data show that the region probed by CO is only a small part of the circumstellar envelope. Indeed, Young et al. (1993a) fit the 60 μm IRAS data with a detached shell of inner radius 2.8′ (or 0.18 pc at 218 pc) and outer radius 5.5′ (0.35 pc). Y CVn has also been imaged with ISO at 90 and 160 μm by Izumiura et al. (1996). The image at 90 μm shows a clear detached dust shell of ∼3′ inner radius. The authors find that the present day mass loss rate is two orders of magnitude smaller than the one obtained for the detached dust shell.

3. Observations

3.1. Observing procedure

The observations have been carried out with the Nançay Radio-Telescope (NRT) between June 2002 and October 2003. With this meridian instrument, a source can be observed for typically one hour at each transit. The beam-width at 21 cm is 4′ in right ascension (RA) and ∼22′ in declination. The beam efficiency, measured on the Moon, is 0.65. The point source efficiency is 1.4 K Jy^{-1} at 21 cm wavelength and the total system noise temperature ∼35 K. The 8192 channel autocorrelator was configured in 4 banks of 2048 channels providing respectively the vertical (PA = 0°) and horizontal (PA = 90°) linear polarisations and the left- and right-handed circular polarisations. For our H I programme, we average the vertical and horizontal polarisations i.e. only consider the Stokes parameter I (total intensity). The separate polarisation channels are systematically recorded to cope with possible radio frequency interferences (RFI) but none was detected throughout our observations, not surprisingly since all H I stellar emissions fall within the radioastronomy protected band 1400.0−1427.0 MHz.

As a first step for each object in our programme, observations are systematically acquired in frequency-switch (f-switch) mode in order to check the level of interstellar H I contamination around the source LSR-velocity, i.e. −34 km s^{-1} in the case of EP Aqr, and +21 km s^{-1} for Y CVn. These data are acquired with a spectral resolution of 0.08 km s^{-1} and a bandwidth of 160 km s^{-1}. The corresponding f-switch spectra are shown in Fig. 1. The brightness temperature of the background interstellar H I emission can be estimated at ∼1 K, in the velocity range of interest ($V_{\rm lsr} \pm 15$ km s^{-1}). Since all our H I candidate sources have been extensively observed in several rotational lines of CO, the central velocity ($V_{\rm lsr}$) and the terminal outflow velocity ($V_{\rm exp}$) are useful to determine the expected velocity range of the H I profiles namely ($V_{\rm lsr} - V_{\rm exp}$, $V_{\rm lsr} + V_{\rm exp}$). Indeed the total H I velocity extent observed on Mira Ceti (BK88), IRC +10216 (Paper I) and RS Cnc (Paper II) well match the total CO velocity extent. Figure 1 readily suggests that there is significant H I emission associated with the circumstellar shells overlaid on the background galactic emission.

Nevertheless, the bulk of the observations are performed in the position-switch mode as our experience has shown that this mode is most effective in subtracting the galactic background H I emission. The spectral resolution is 0.04 km s^{-1} and the bandwidth, 80 km s^{-1}. The data are binned with a boxcar to give a spectral resolution of 0.16 km s^{-1} and then Hanning-smoothed. The off-positions are usually taken at ±1 NRT beam (i.e. 4′) and ±2 NRT beam (i.e. 8′) in the east-west direction. The symmetrical east-west off-positions are usually averaged to yield the mean off-position i.e. the expected off profile at the source position that one would have found without the star. If the galactic H I background has a linear brightness temperature gradient across the source, then this procedure should totally remove the confusion. But this procedure will also subtract genuine emission from the envelope that may be contained in the off-positions. Indeed, in the two cases discussed in this paper, we found significant differences between the (on–off) spectra obtained with reference positions at ±4′ and 8′ (see Figs. 2 and 6). Therefore, more spectra were acquired with larger beam-throws; also we explored the north–south dependence by steps of 11′ (see Sects. 3.2 and 3.3).

Drift scans on the radio-continuum sources 3C 295, 3C 161 and 3C 286, centered on the sources and then at ±1/2 lobe and ±1 lobe in the north–south direction (i.e. ±11′ and ±22′), show that the NRT beam at 21 cm has secondary lobes at a level

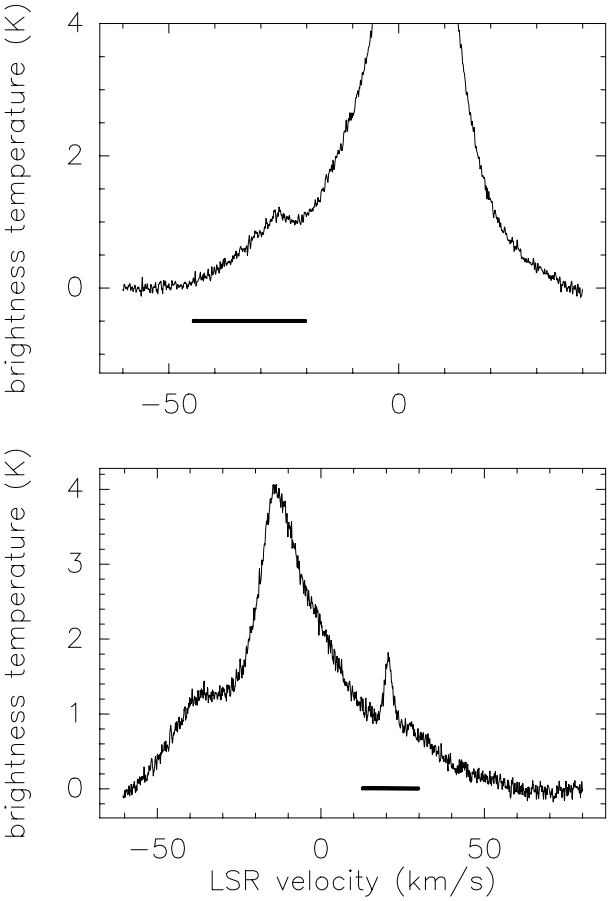

Fig. 1. On-source spectra obtained in f-switch mode; *upper panel*: EP Aqr, *lower panel*: Y CVn. The emission comes essentially from interstellar atomic hydrogen on the line of sight. However one may see the H I emission from the CS of EP Aqr at ∼−30 km s^{-1} and of Y CVn at +21 km s^{-1}; the bars mark the velocity spread corresponding to the CO emission.

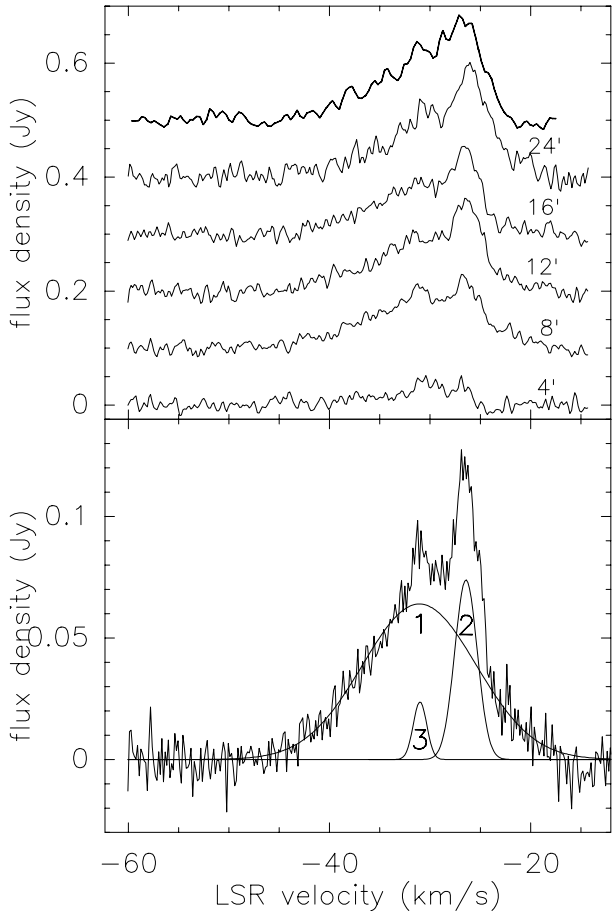

Fig. 2. *Upper panel*: EP Aqr spectra obtained in the position-switch mode with the source centered ("on") and the off-positions taken in the east-west direction at ±4′, ±8′, ±12′, ±16′ and ±24′ (thin lines), and the baseline-subtracted f-switch spectrum (thick line). For clarity the spectra are successively shifted upwards by 0.1 Jy and labelled with the corresponding offsets. *Lower panel*: average of the 5 position-switch spectra presented in the upper panel without Hanning smoothing.

of ≤5% in both directions, as expected from an un-obstructed rectangular aperture (theoretical value: 0.045).

3.2. EP Aqr

The spectra obtained with the source positioned in the central beam ("on") and the off-positions placed symmetrically at ±4′, ±8′, ±12′, ±16′ and ±24′ in the east-west direction are presented in Fig. 2 (upper panel). One notes that, with the off-positions at ±4′, the signal is much weaker than with the off-positions at ±8′. On the other hand, the spectra with the off-positions at ±16′ and ±24′ are quite similar and give a peak intensity comparable to what one would expect from the f-switch spectrum shown in Fig. 1. This is illustrated in Fig. 2 (upper panel) where the f-switch spectrum has been corrected with a third-order baseline fitted to the velocity ranges (−60, −45 km s^{-1}) and (−12, −30 km s^{-1}) and corrected for a point source efficiency of 1.4 K Jy^{-1}.

The source is clearly extended in the east-west direction, but does not seem to reach much further than ±10′ in that direction. This is however considerably more than expected from the CO data (see Sect. 2.1) and even still larger than expected from the IRAS data. We stress that a simple search with comparison positions taken at only ±4′ would have missed most of the H I flux. At a distance of 135 pc, the NRT beam scales as 0.16 pc in RA and 0.86 pc in declination while the 21-cm source-size ranges between 12′ (0.5 pc) and 20′ (0.8 pc).

Table 1. Gaussian fits to the three components of the H I emission from EP Aqr as represented in Fig. 2 (lower panel).

	$V_{\rm cent.}$	*FWHM*	$F_{\rm peak}$
	km s^{-1}	km s^{-1}	mJy
Comp. 1	−31.06	13.34	64
Comp. 2	−26.43	2.62	73
Comp. 3	−30.99	1.59	24

The inspection of these spectra leads us to identify three components in the H I profile (Fig. 2, lower panel). The strongest one (hereafter Comp. 2) is centered at −26 km s^{-1} and can be well fitted with a Gaussian (Table 1[1]). The two other features are centered at ∼−31 km s^{-1}, and are reminiscent of those observed in CO, i.e. a narrow one of width ∼2 km s^{-1} (Comp. 3), and a broad one of width ∼13 km s^{-1} (Comp. 1). They can be fitted with Gaussians (Table 1); however we note that Comp. 3 could be fitted as well with a rectangular profile (see Fig. 10). This situation is similar to the one in RS Cnc (Paper II). The amplitude and width of the narrow feature (3) seem stable versus beam-throw, which indicates that the gas responsible for it is concentrated in the central beam. This is not the case for the 2 broader features (1 and 2) and therefore the evidence of extension seen in Fig. 2 can be ascribed to them essentially. Finally, we note that the two features at −31 km s^{-1} (1 and 3) are slightly shifted in velocity w.r.t. the CO features which are rather centered at −34 km s^{-1} (e.g. Winters et al. 2003). We have no reason to suspect an error in the frequency scales and believe that this velocity shift is real. Also we have several cases in our sample of AGB sources for which we noted a shift (positive or negative) of ∼1−2 km s^{-1} (Gérard & Le Bertre, in preparation). For example, for RS Cnc, in H I (Paper II) we get a shift of ∼−1 km s^{-1} w.r.t. CO (Knapp et al. 1998). As discussed in Sect. 4.2, there are several reasons why the velocities in H I and CO might not be exactly the same.

We have also reduced our position-switch data by considering the two off-positions separately to test our hypothesis that the H I galactic background varies linearly across the source. To this end, we subtract the off-spectrum obtained at $n \times 4'$ east from the one obtained at $n \times 4'$ west, and normalize the difference by n, for n = 1, 2, 3, 4 and 6. The results are shown in Fig. 3. The spectra are quasi-identical in the velocity range −70 to −30 km s^{-1} and around −15 km s^{-1}. The agreement degrades rapidly at velocities close to 0 km s^{-1} where the background signal is the strongest (see Fig. 1). The features at −31 km s^{-1} (1 and 3) are hardly visible, but surprisingly the

[1] For the decomposition we used the data without Hanning smoothing.

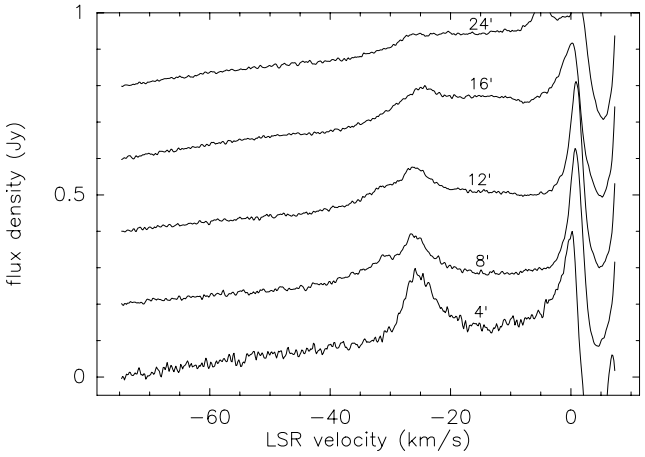

Fig. 3. Differences between the two reference spectra obtained at ±4′ in RA from EP Aqr, ±8′, ±12′, ±16′ and ±24′, and normalized by 1, 2, 3, 4 and 6, respectively. For clarity the spectra are successively shifted upwards by steps of 0.2 Jy and labelled with the corresponding offsets.

feature at −26 km s^{-1} (2) stands out clearly. This means that the features at −31 km s^{-1} (1 and 3) are approximately centered in RA w.r.t. EP Aqr, but not that at −26 km s^{-1} (2). As the intensity of the latter decreases with n, we can estimate that it should be centered at ∼1−2 lobes (4−8′) west of EP Aqr (see also, below, Fig. 5). We note that asymmetries in the H I emission distribution are also present in several other sources of our sample (Gérard & Le Bertre, in preparation) and that an asymmetry is present also in the north-south direction of EP Aqr (see below).

Finally we explored the H I brightness distribution north and south by repeating the same east-west position-switch technique with steps of 1/2 NRT lobe (i.e. 11′) between one beam north (+22′) and two beams south (−44′). The results are presented in Fig. 4 for a beam-throw (east-west) of 12′. In the north-south direction we have also evidence of an asymmetry, the broad feature at −31 km s^{-1} (1) being stronger south; the maximum probably lies at ∼1/2 lobe (11′) south of the stellar position of EP Aqr. We infer that, for this feature, as for the −26 km s^{-1} one (2), the peak of the H I emission is not exactly coincident with the central star. This emission is larger for a beam throw of 8′ than for a throw of 4′. The H I emission corresponding to the broad feature at −31 km s^{-1} (1) is therefore extended in RA over ∼12′. Almost no signal was detected at two beams south and one beam north of EP Aqr, setting an upper limit of 33′ for the extension from the stellar position. Figure 4 also suggests that the peak of the H I emission at −26 km s^{-1} (2) is slightly offset to the north (see also Fig. 5).

The position-switch spectra obtained for various beam-throws and at several positions north and south reveal that the spatial variation of the 21 cm emission is complex and that the shape of the line-profile varies with position. To illustrate these effects, we have extracted the H I-profile at each position on the sky by assuming that the most distant off-positions are devoid of circumstellar emission and that the galactic background varies linearly across the field of EP Aqr. The resulting "map" (Fig. 5) contains 31 H I-profiles, separated by steps of 4′ in RA (i.e. 1 beam) and 11′ in Dec (1/2 beam). This map

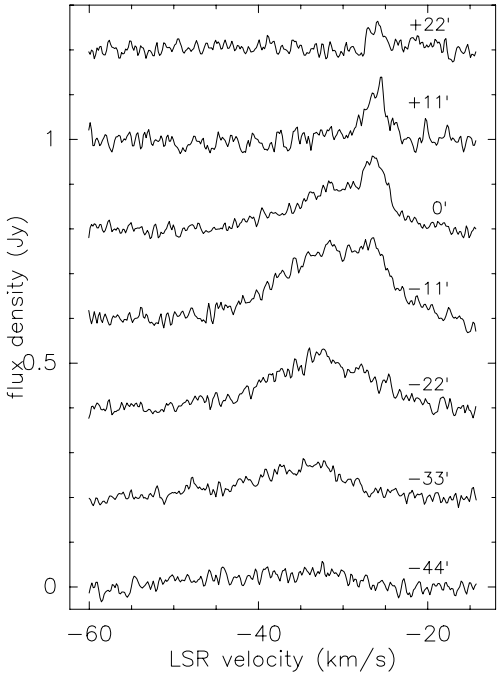

Fig. 4. From top to bottom: position-switch spectra for EP Aqr with the central beam placed at +22′ in declination, +11′, on source, −11′, −22′, −33′ and −44′. The off-positions are taken at ±12′ in RA. For clarity the spectra are successively shifted by steps of 0.2 Jy and labelled with the corresponding positions in declination.

suggests that the broad emission at −31 km s^{-1} (1) traces a large structure starting from the center (i.e. the optical position of EP Aqr) and extending to the south-east. The broad emission at −26 km s^{-1} (2) seems to develop along a wide arc peaking west and enclosing the central position. Obviously a map with a better spatial resolution would be needed to reveal the true structure of the EP Aqr circumstellar environment.

A total of 65 h of integration has been acquired on this source (on + off).

3.3. Y CVn

We have applied the same observational strategy for Y CVn. The position-switch spectra acquired with the source centered are shown in Fig. 6 (upper panel). About half of the flux density is seen at ±4′. The spectra with off-positions at ±8′ are basically identical to those with off-positions at ±12′ and ±16′. The f-switch spectrum (Fig. 6, upper panel) has been corrected with a third order baseline fitted to the velocity ranges (0, 12 km s^{-1}) and (30, 40 km s^{-1}). The comparison with the f-switch spectrum confirms that most of the signal has been recovered at ±8′. As the interstellar emission is quite low in the direction of Y CVn, we could also take a spectrum with the off-positions at ±8 lobes (i.e. ±32′); we find no significative difference with respect to the previous spectra.

The source is extended but somewhat less than EP Aqr; we estimate its size to ≤12′, in good agreement with the IRAS and ISO results. At the distance of Y CVn (218 pc), the NRT beam scales as 0.25 pc in RA and 1.40 pc in Dec, while the size of the source is of the order of 0.8 pc.

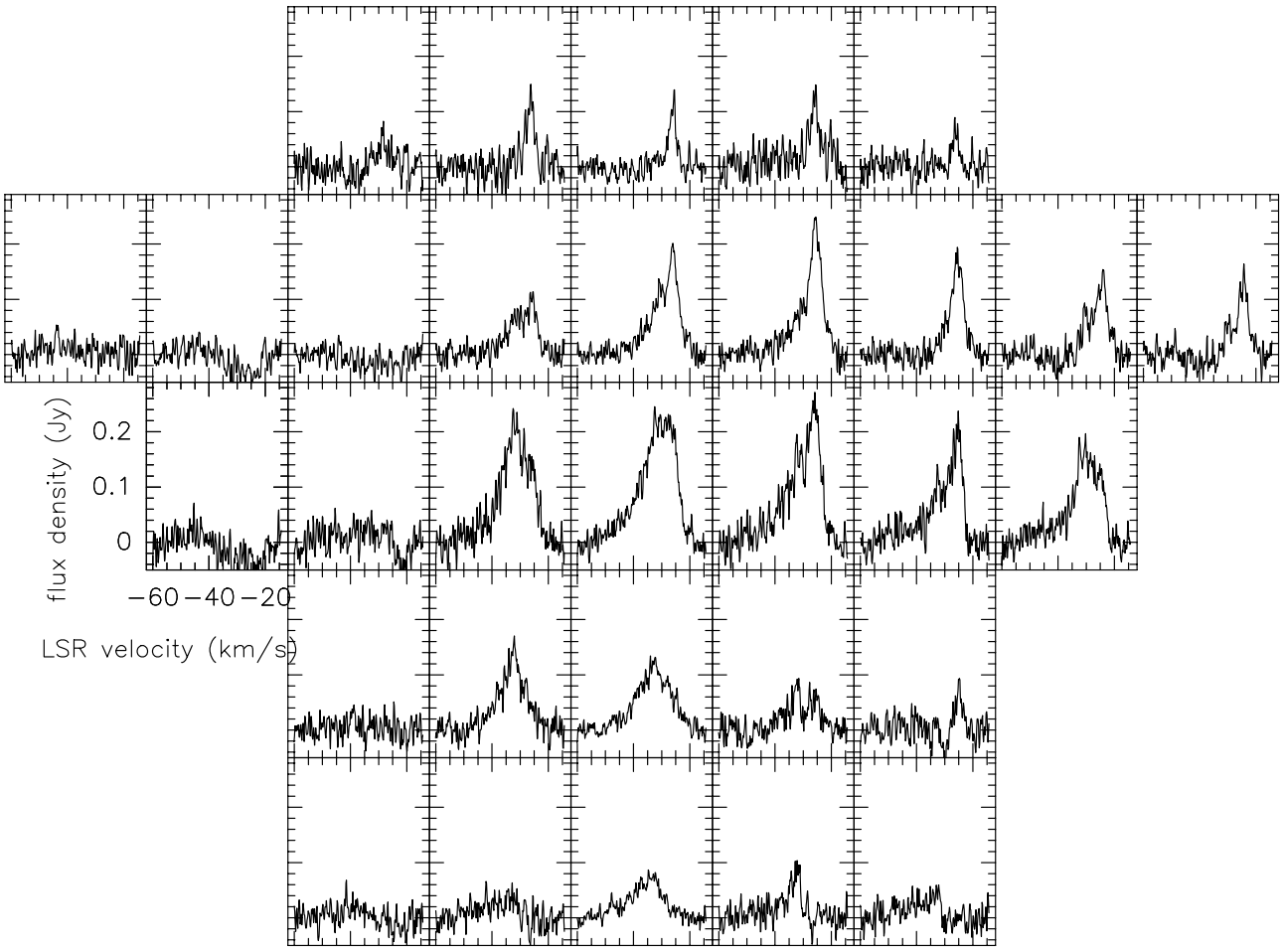

Fig. 5. Map of the 21 cm H I emission from the EP Aqr circumstellar envelope observed with the NRT. The central position in the second row from the top corresponds to the star; the steps are 4′ in RA and 11′ in declination. North is up and east to the left. Almost no signal was detected in the rows at 22′ north and 44′ south of EP Aqr (see Fig. 4).

The H I profile is dominated by a narrow component of width ∼3 km s^{-1} which is superimposed on a broad one of width ∼20 km s^{-1} (Fig. 6, lower panel). Both components can be fitted with Gaussians (Table 2). The broad feature (Comp. 2) seems stable with beam-throw, in contrast to the narrow one (Comp. 1) whose amplitude clearly increases with beam-throw. This indicates that the angular extension of the source is mainly the effect of the narrow feature (1). The broad component (2) can be associated to the feature observed in the CO rotational lines whose width is ∼16−20 km s^{-1} (Neri et al. 1998; Knapp et al. 1998, 2000). However there is no evidence in the CO spectra of a counterpart to the H I narrow-feature (1). Probably, the material responsible for it is at a distance from the central star such that CO has completely disappeared due to photo-dissociation. The spatial extension of this component corresponds to the far-infrared emission seen by IRAS and ISO, which also has no CO counterpart. Furthermore the ISO data at 90 μm show a detached shell with inner radius ∼1.5′, larger than the observed photo-dissociation radius of CO (Neri et al. 1998).

As for EP Aqr we have also reduced our position-switch data by considering the two off-positions separately (Fig. 7). One sees an asymmetry for a throw of 4′, which is also present but at a much smaller level for a throw of 8′. However, although the amplitudes of the narrow component (1) seen at +4′ and −4′ differ by a factor 2 (350 mJy and 150 mJy, resp., see Fig. 9), the central velocities and the widths stay the same. Furthermore, the central velocities are the same as the LSR velocity of Y CVn (see e.g. Knapp et al. 1998). Therefore we are confident in ascribing the narrow feature (1) also to the Y CVn outflow and we conclude that it presents some asymmetry at a scale of ∼4′. We note that this asymmetry tends to disappear at a scale of ∼8′ (410 and 380 mJy, resp.). Furthermore, when the spectra at ±12′ and ±16′ are also reduced separately, no difference is observed. It confirms that the position-switch procedure is effective in separating the Y CVn H I emission from the interstellar one. All this strengthens the assignment of the whole emission to Y CVn.

We also took spectra in the position-switch mode with the "on" position at ±1/2 NRT lobe (i.e. 11′) and at ±1 lobe (22′) in the north-south direction (Fig. 8). We did not found any significative evidence of an asymmetry in this direction. Of course this should be handled with caution as the signal decreases rapidly when we move away from the source; for instance at 22′ north or south from Y CVn, with off-positions at ±12′ (east-west), the peak intensity is only ∼60 mJy.

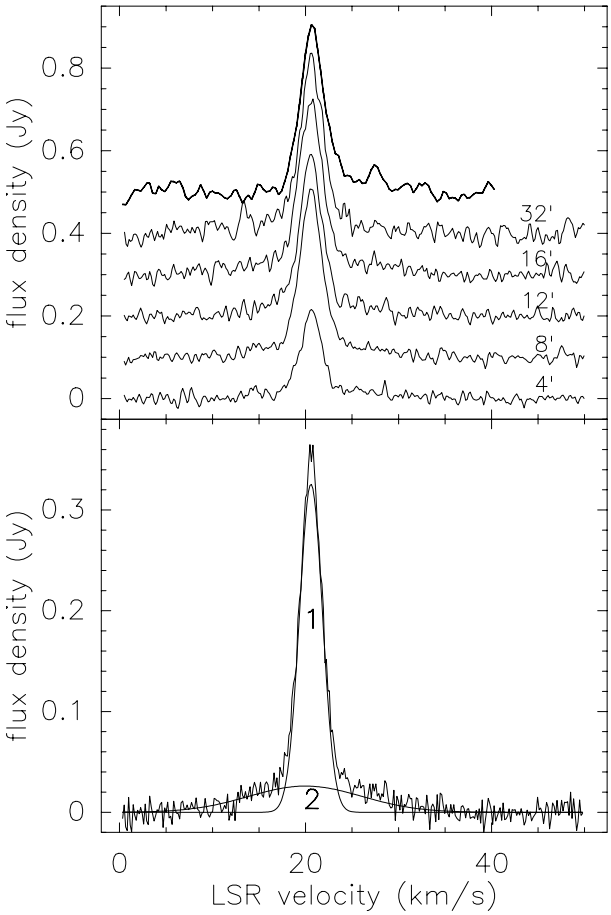

Fig. 6. *Upper panel*: Y CVn spectra obtained in the position-switch mode with the source centered ("on") and the off-positions taken in the east-west direction at ±4′, ±8′, ±12′, ±16′ and ±32′ (thin lines), and the baseline-subtracted f-switch spectrum (thick line). For clarity the spectra are successively shifted upwards by steps of 0.1 Jy and labelled with the corresponding offsets. *Lower panel*: average of the 5 position-switch spectra presented in the upper panel without Hanning smoothing.

Table 2. Gaussian fits to the two components of the H I emission from Y CVn as represented in Fig. 6 (lower panel).

	$V_{\rm cent.}$	*FWHM*	$F_{\rm peak}$
	km s^{-1}	km s^{-1}	mJy
Comp. 1	20.58	2.91	325
Comp. 2	19.97	14.33	26

Finally, as for EP Aqr, we have constructed a "map" of the H I emission around Y CVn by assuming that the most distant off-positions are devoid of circumstellar emission and that the galactic background varies linearly across the field of Y CVn. The resulting "map" (Fig. 9) contains 29 H I-profiles.

A total of 52 h of integration has been acquired on this source.

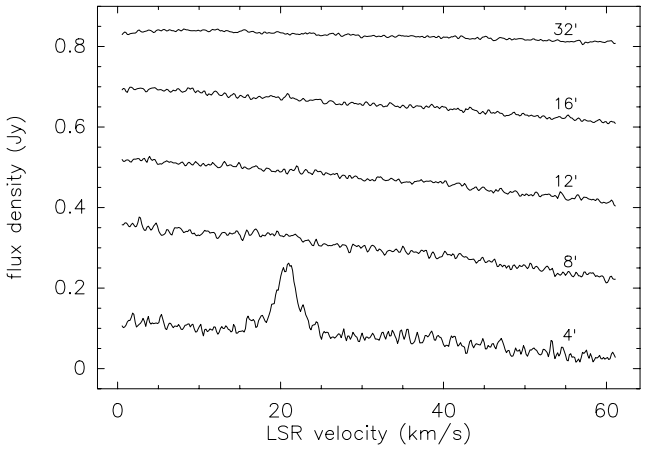

Fig. 7. Differences between the two reference spectra obtained at ±4′ in RA from Y CVn, ±8′, ±12′, ±16′ and ±32′, and normalized by 1, 2, 3, 4 and 8, respectively. For clarity the spectra are successively shifted upwards by steps of 0.2 Jy and labelled with the corresponding offsets.

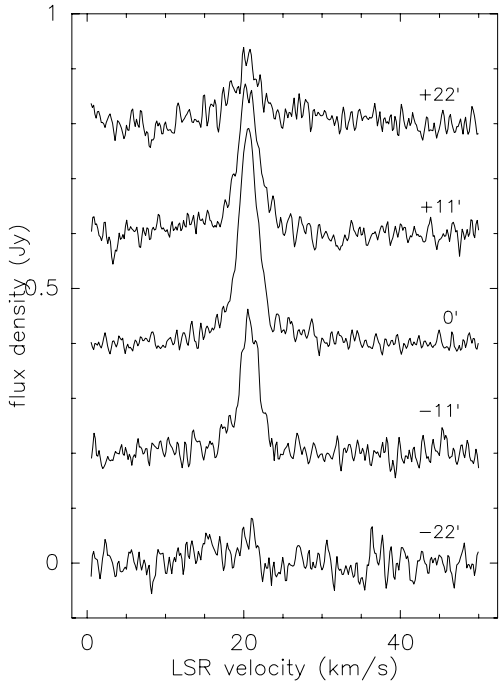

Fig. 8. From top to bottom: position-switch spectra for Y CVn with the central beam placed at +22′ in declination, +11′, on the source, −11′ and −22′. The off-positions are taken at ±12′ in RA. For clarity the spectra are successively shifted by steps of 0.2 Jy and labelled with the corresponding positions in declination.

4. Interpretation

4.1. Introduction

The two H I sources discussed in this paper are clearly spatially extended w.r.t. the NRT beam (4′).

Rodríguez et al. (2002) have obtained H I images of the planetary nebula NGC 7293 with the Very Large Array (VLA). The material seen in H I most likely was expelled from the central star when it was a red giant. Therefore it can be considered as an expanded paradigm of the past circumstellar environment

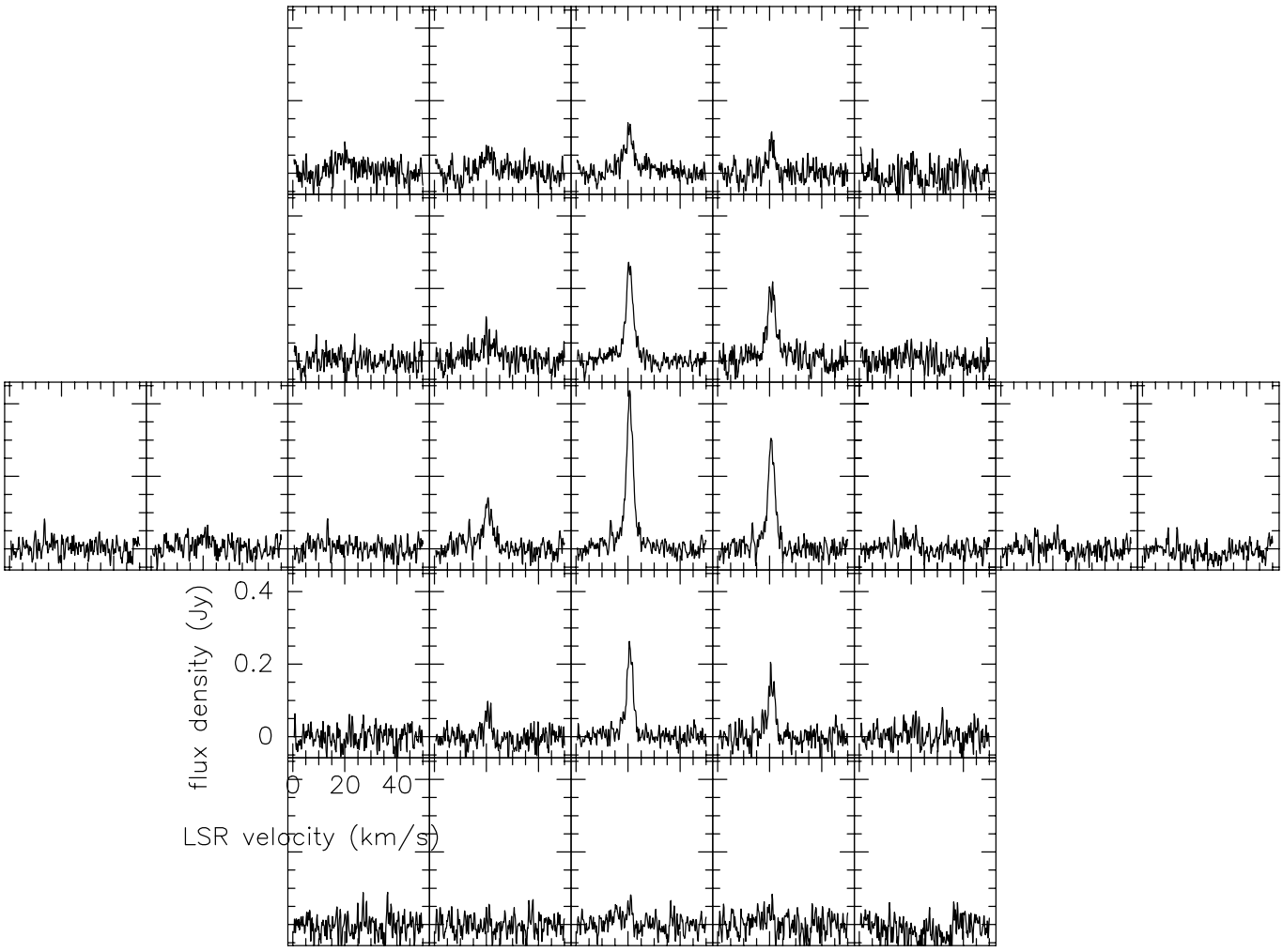

Fig. 9. Map of the 21 cm H I emission from the Y CVn circumstellar envelope observed with the NRT. The central position in the third row corresponds to the star; the steps are 4′ in RA and 11′ in declination. North is up and east to the left.

of this red giant. Of course this material has been subject to mechanical and radiative alterations from inside as well as from outside. The velocity-integrated image shows shells which are fragmented with large gaps. The fragments are seen at different velocities. Young et al. (1999) have obtained maps in CO of the same neutral environment. These show also fragments of shells at different velocities. Interestingly, for H I and CO fragments which are at the same location on the maps, the velocities may differ; this is probably an effect of the complex 3-dimensional structure of the environment (Huggins et al. 1999).

4.2. EP Aqr

The three H I components have a velocity spread which fits within the velocity range of the CO broad feature (−45 to −20 km s^{-1}, Winters et al. 2003). The narrow component at −31 km s^{-1} (3) is centered on the optical position of EP Aqr and unresolved w.r.t. the NRT beam (4′). The two broad components (1 and 2) are offset w.r.t. to the optical/CO position, but overlap with the extended IRAS source. We stress that, in spite of these offsets, they are present in the f-switch spectrum obtained directly on the source (upper panel of Fig. 2). Furthermore the broad component at −31 km s^{-1} (1) is centered at the same velocity as the narrow component (3), and the second broad component, at −26 km s^{-1} (2), has a counterpart in CO (Fig. 11 in Winters et al. 2003). Finally, we note that the thermal SiO emissions detected by González Delgado et al. (2003) are centered at −32 km s^{-1}, i.e. between the CO and H I central velocities (1 and 3). For all these reasons, we ascribe the three H I components to the outflow from EP Aqr.

The narrow feature at −31 km s^{-1} (3) can be easily extracted by subtracting the two broad features (1 and 2) from the position-switch spectra presented in Fig. 2. The result is presented in Fig. 10 together with a Gaussian fit of width 1.6 km s^{-1} and intensity 0.024 Jy and a rectangular fit of width 2 km s^{-1} and intensity 0.020 Jy. The corresponding mass of atomic hydrogen in the central beam is $\sim 2 \times 10^{-4} \pm 3 \times 10^{-5}$ $M_\odot$ (d = 135 pc). (This procedure is valid only if the gas responsible for component 3 is concentrated in the central beam.) From this estimate, and assuming a spatial extension of 4′, we can derive a lower limit on the mass loss rate in atomic hydrogen for the corresponding outflow of $\sim 3 \times 10^{-9}$ $M_\odot$ yr^{-1}. This limit is compatible with the estimates obtained from CO, $\sim 3 \times 10^{-8}$ $M_\odot$ yr^{-1} (Knapp et al. 1998;

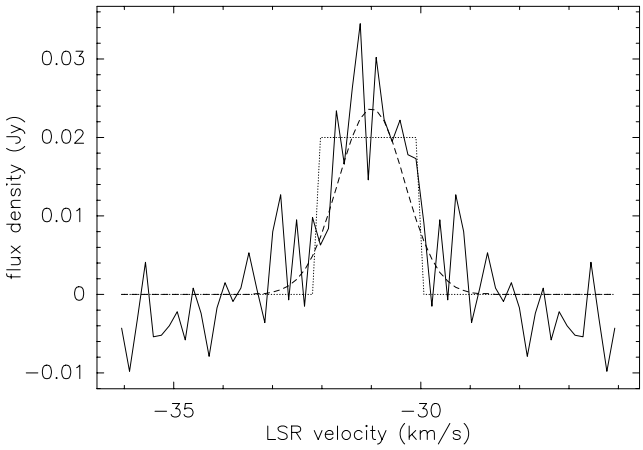

Fig. 10. The EP Aqr narrow feature. A Gaussian fit is shown as a dashed line and a rectangular one, as a dotted line.

Olofsson et al. 2002; Winters et al. 2003) for the total mass loss rate. However we caution that a direct comparison might not be warranted because the CO and H I narrow features do not overlap perfectly in velocity.

The total hydrogen masses corresponding to components 1 and 2 have been estimated by integrating the flux density under the profiles displayed in Fig. 5. We find respectively ∼0.031 ± 0.003 $M_\odot$ and ∼0.015 ± 0.002 $M_\odot$.

Most of the H I emission found in the direction of EP Aqr and in the velocity range (−45, −20 km s^{-1}) can be attributed to the two broad components centered at −31 and −26 km s^{-1} (Sect. 3.2). The first component (1) appears displaced to the south (perhaps south-east, see Fig. 5), and the second one (2) to the west (north-west?). This could be an indication of a bipolar flow as in X Her (Kahane & Jura 1996). However, we think that, in the present context, this hypothesis is unlikely because both features are red-shifted with respect to the CO emission which is centered at ∼−34 km s^{-1} (Knapp et al. 1998; Winters et al. 2003). A possibility could still be that the −26 km s^{-1} feature represents the red-shifted component of a very asymmetric bipolar flow whose blue-shifted component would be much weaker and not detected in H I. Another hypothesis, that we favour, would be that we see fragments of an expanding shell as the NGC 7293 H I-image suggests. In fact we cannot exclude that these two components (1 and 2) trace a large structure that would include both of them and for which the radial velocity would change gradually with position. Obviously a mapping with a better spatial resolution is needed to clarify this issue.

However, contrary to what Rodríguez et al. (2002) find in NGC 7293, we detect H I at the location of the central star. The three components contribute to the emission in the central position. In particular the narrow component at −31 km s^{-1} (3) is centered on it. The velocity shift between the H I narrow feature and the CO one is real. It is worth noting that the H I and CO features are so narrow that there is basically no overlap in velocity between them. It is noteworthy also that the CO narrow feature in EP Aqr is the narrowest among those reported by Knapp et al. (1998) and Winters et al. (2003). To our knowledge only one narrower case has been reported in the literature by Kahane et al. (1998) for BM Gem, a carbon star

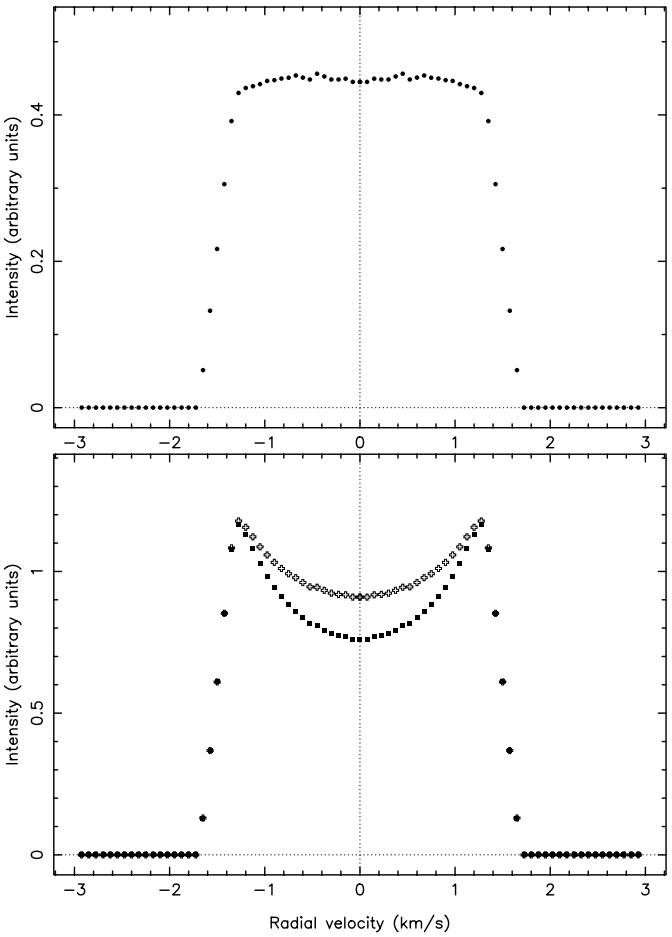

Fig. 11. Simulation of the H I emission profile, observed with the NRT in the position-switch mode, for a spherically symmetric outflow of constant velocity, $V_{\rm exp}$ = 1.5 km s^{-1}, and a constant H I-production rate. *Upper panel*: the external limit of the outflow is at 1.5′ from the center. *Lower panel*: the external limit is at 4′; filled symbols: off-positions at ±4′, empty symbols: off-positions at ±8′.

associated to an oxygen-rich circumstellar environment. In this case it appears that the emission corresponding to the CO narrow feature arises in a circumbinary reservoir, not in an outflow.

We observe almost the same velocity shift between the H I broad component at −31 km s^{-1} (1) and the CO broad feature. These shifts are intriguing, but not totally unexpected. Indeed they may be the effect of the different beams used for CO and H I observations. A concentration of material ("cloud") with an angular size comparable to the CO beam (less than 1′) will be diluted within the NRT H I-beam, and inversely clouds which fit within the H I-beam may fall outside the CO-beam. Furthermore some clouds may contain H I, but not CO, if the latter has been photo-dissociated. Inversely some clouds may contain only molecular hydrogen. In other words CO and H I may not necessarily co-exist spatially and kinematically, a fact which is illustrated by the comparison between the H I map of NGC 7293 (Fig. 7 in Rodríguez et al. 2002) and the CO map (Fig. 4 in Young et al. 1999). Finally, the velocity differences between CO and H I features may also come from a complex velocity field in the outflow.

4.3. Y CVn

The H I emission from Y CVn is dominated by its narrow component (1) which is extended w.r.t. the NRT beam (4′) and has a Gaussian profile of width 3 km s^{-1} and maximum intensity 300 mJy. The emission is almost symmetrical and centered on the optical counterpart. In the following we assume a spherical symmetry. This hypothesis is also supported by the ISO images (Izumiura et al. 1996). The total hydrogen masses corresponding to components 1 and 2 have been estimated by integrating the flux density under the profiles displayed in Fig. 9. We find respectively ∼0.029 ± 0.001 $M_\odot$ and ∼0.015 ± 0.002 $M_\odot$ in atomic hydrogen.

The H I narrow-component (1) properties distinguish it from the narrow feature observed in EP Aqr and in RS Cnc (Paper II). To investigate this difference we have made simulations of the H I emission pattern produced by a spherically symmetric outflow and observed with the NRT in the position-switch mode. We first assume a constant outflow velocity and a constant production rate of atomic hydrogen, (Fig. 11). As long as the maximum extension of the outflow is smaller than the width of the beam, the profile is rectangular. A rectangular line-profile is a general result for a wind in radial expansion at constant velocity, in the case of an optically thin emission and an unresolved source. When the outflow extends beyond the beam, a deficit appears in the center of the profile. This is because some particles flowing out in a direction perpendicular to the line of sight do not contribute to the emission at velocities close to $V_{\rm lsr}$, or even contribute negatively if they happen to be detected in the off-positions (see lower panel of Fig. 11). Isotropic outflows with constant velocity which are spatially resolved should therefore be characterized by the presence of two horns at $V_{\rm lsr} - V_{\rm exp}$ and $V_{\rm lsr} + V_{\rm exp}$. In our programme we never observed such a profile. We only get quasi-rectangular, or Gaussian profiles, or a mixture of the two (Gérard & Le Bertre, in preparation).

Quasi-Gaussian profiles can be obtained for outflows with different expansion velocities. This may happen if the central star undergoes a succession of mass loss episodes with different characteristics. Such a situation may also result from the interaction of the stellar wind with the ISM, (Lamers & Cassinelli 1999). To illustrate this, we replace the constant outflow velocity by a velocity decreasing linearly with radius. Of course there is no supporting hydrodynamical model for such a law, but our purpose is only to explore the dependence of the H I profile on the kinematics. In the upper panel of Fig. 12, we show the results of such a simulation in the case of an unresolved source. However for a source which is angularly resolved, we expect again a deficit in the center of the profile (Fig. 12, lower panel), unless there is an important quantity of atomic hydrogen at zero velocity along the line of sight. This may happen in the case of the interaction with the ISM for stellar winds which have been outflowing for long periods of time, typically ≥10^5 years (Young et al. 1993b). The ISM material swept-up by the stellar outflow is added to the compressed and slowed-down circumstellar material. In Fig. 13 the velocity is chosen to decrease down to ∼zero (for numerical reasons, the final velocity cannot be set exactly to 0 km s^{-1}).

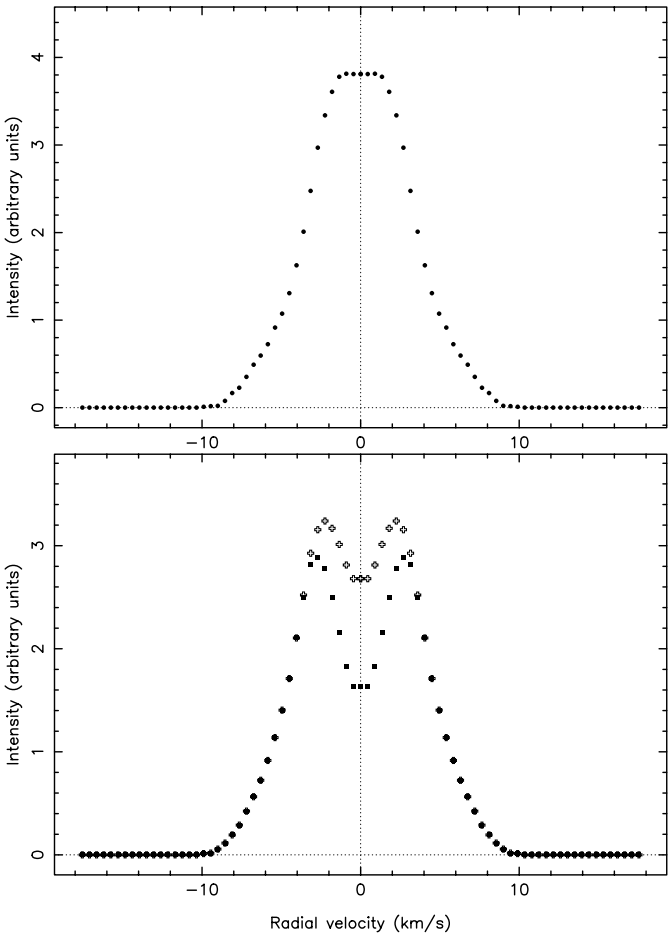

Fig. 12. Simulation of the H I emission profile, observed with the NRT in the position-switch mode, for a spherically symmetric outflow with a velocity decreasing linearly, from $V_{\rm exp}$ = 9 km s^{-1} to 1/4 × $V_{\rm exp}$ at the outer boundary, and a constant H I-production rate. *Upper panel*: the external limit of the outflow is at 1.5′ from the center. *Lower panel*: the external limit is at 4′; filled symbols: off-positions at ±4′, empty symbols: off-positions at ±8′.

Therefore the presence of an extended H I emission with a narrow profile could be due to a long-duration interaction between the stellar wind from Y CVn and its surrounding ISM.

To reproduce the H I profile of Y CVn we invoke two shells with outflow velocity decreasing with distance from the central star. An example is shown in Fig. 14. For simplicity we have assumed a constant H I flux, i.e. $\rho_{\rm HI}\ v_{\rm HI}\ r^2$ = constant, and adopted the same constant value for the two shells. The parameters selected for this simulation are arbitrary and other selections could reproduce such a composite H I profile. For the detached shell it is essential that the outflow velocity decreases with increasing distance. Also for this detached shell, it is important to have a density profile decreasing less rapidly than $1/r^2$, and even increasing with r at the outer boundary.

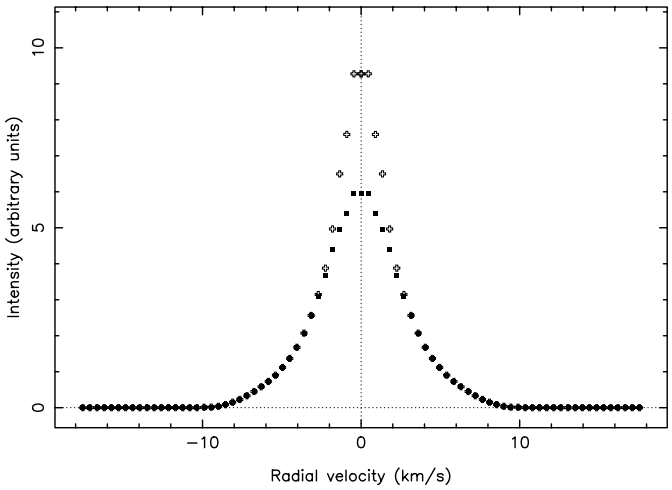

Fig. 13. Simulation of the H I emission profile, observed with the NRT in the position-switch mode, for a spherically symmetric outflow with a velocity decreasing linearly, from $V_{\rm exp}$ = 9 km s^{-1} to 1 km s^{-1} at the outer boundary, and a constant H I-production rate. The external limit is at 4′; filled symbols: off-positions at ±4′, empty symbols: off-positions at ±8′.

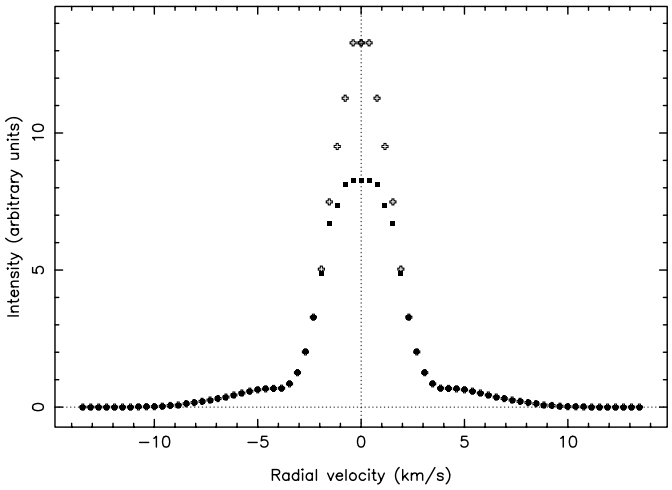

Fig. 14. Simulation of the H I emission profile, observed with the NRT in the position-switch mode, for a spherically symmetric outflow with 2 components: (i) a circumstellar shell with outflow velocity decreasing linearly from $V_{\rm exp}$ = 10 km s^{-1} to 5 km s^{-1} at 1.5′; (ii) a detached shell of inner radius 2.0′, outer radius 4.0′ and an outflow velocity decreasing linearly from 3 km s^{-1} to 0.6 km s^{-1}; filled symbols: off-positions at ±4′, empty symbols: off-positions at ±8′.

5. Discussion

5.1. Observing circumstellar H I at 21 cm

The observations that we have presented and the detailed analysis of our data allow us to comment on the difficulties that one may face when observing circumstellar H I at 21 cm.

An inherent difficulty is the contamination by galactic H I ("confusion"). It is not only the effect of interstellar gas on the line of sight, but also it may be due to gas surrounding the source. We note that the latter may be related to the source in several ways: this gas may come from mass loss during a previous stage of evolution (e.g. when the star was on the first Red Giant Branch) or it may be interstellar gas interacting with the circumstellar outflow.

Another difficulty, specific to the nearby sources (≤500 pc) that we have observed, is that the H I shell extension may be so large that it is resolved by the NRT. Our data show that H I shells may easily reach sizes ∼1 pc.

We have performed observations in the f-switch mode and in the position-switch mode. The advantage of the former is that all H I emission is detected. The drawback is that the line profile is complex and requires a second or third-order baseline fit in order to isolate the circumstellar emission, a delicate operation especially when the confusion level is high (>1 K). In this respect the position-switch mode is better because it acts as a spatial filter which is efficient in removing the confusion. The obvious drawback is that, when the source is extended, a part of its emission is also filtered. The case of EP Aqr (Fig. 2) is particularly spectacular. To fully recover the signal, we had to take off-positions at ±16′ and more, with the drawback that the confusion may not be so well removed if it does not vary linearly across the sky. One clearly sees the need for an interferometer providing a bidimensional map over a large field of view (>1 degree) and thus giving access to the galactic background emission well outside the circumstellar source.

Finally, we find that the circumstellar H I emission may be irregularly distributed with peaks, at some velocities, offset w.r.t. the central star. Pointed observations are clearly insufficient.

The confusion problem, the large extension on the sky of the H I emission and its irregular distribution may explain in part why previous searches were largely unsuccessful.

5.2. EP Aqr

The extent of the H I emission from EP Aqr is very large on the sky, even larger than that of the IRAS emission at 60 μm. It corresponds to a ∼1 pc shell enclosing ∼0.062 $M_\odot$ of circumstellar matter (assuming all hydrogen is atomic and accounting for 25% in He). Adopting an average expansion velocity of 6 km s^{-1}, the timescale to build such a shell is $\sim 1.6 \times 10^5$ years and the average mass loss rate over this timescale is $\sim 4 \times 10^{-7}\ M_\odot\,{\rm yr}^{-1}$. This is comparable to what Knapp et al. (1998), Olofsson et al. (2002) and Winters et al. (2003) estimate for the high velocity wind detected in CO. The detail of the history of mass loss over the past 1.6×10^5 years requires a better spatial resolution than the one provided presently by the NRT.

5.3. Y CVn

From a careful modelling of various CO rotational lines observed in Y CVn, Dinh-V-Trung & Nguyen-Q-Rieu (2000) concluded that the mass loss rate must have increased by a factor 2 or more over the last 1600 years. This may be in contradiction with our interpretation that the outflow velocity should decrease outward. However, we note that the timescales are very different. For an 8 km s^{-1} velocity, which is probably an overestimate of the H I average velocity, the expansion time

corresponding to the broad H I feature is $\sim 15 \times 10^3$ years, or ten times as much as the lapse considered by Dinh-V-Trung & Nguyen-Q-Rieu. Furthermore, in our numerical simulations we need a velocity gradient for both shells, but, strictly speaking, it needs to be negative only for the exterior shell. Obviously a better spatial resolution at 21 cm is needed.

The circumstellar shell of Y CVn was imaged by ISO at 90 and 160 μm (Izumiura et al. 1996). The data show clearly a detached shell. Izumiura et al. estimate the mass loss rate needed for the formation of this shell to $(7-20)\times 10^{-6}\ M_\odot\ \mathrm{yr}^{-1}$, the duration for the event to 10^4 years and the total mass in the shell to $(4-14)\times 10^{-2}\ M_\odot$. The latter is in agreement with our estimate from H I (Sect. 4.3). Nevertheless, in their model they assume a 15 km s^{-1} outflow velocity, which is 10 times as much as what we observe in H I. Therefore the average flux of matter in the detached shell has to be decreased by a factor 10. However, as the duration has to be increased by the same factor, the estimate of the total amount of matter stays the same! Still we caution that in the formation process of the detached shell the circumstellar material may have been augmented by swept-up interstellar matter.

5.4. H I in LPVs

Both sources are clearly detected in H I. They are resolved and are much larger than the CO sources. Therefore atomic hydrogen appears as a major constituent of these circumstellar shells. In Y CVn it is probably present up to the interface with the ISM. This provides a confirmation that it is not easily ionized by the ISRF and that the 21-cm line emission can be used as a probe of circumstellar shells on large scales. It is now clear that imaging of atomic hydrogen at high spatial-resolution with high spectral-resolution ($\leq$1 km s^{-1}) will bring unique informations on the mass loss history of LPVs and on the interaction between their outflows and the ISM. The view on CSs given by H I appears complementary to that provided by the rotational lines of CO which probe only their interiors ($\leq 10^{17}$ cm).

Both stars have an effective temperature larger than 2500 K. Therefore following GH83 we may consider that all hydrogen **presently** leaving the stars is in atomic form. However this may not have always been the case, and part of the atomic hydrogen observed at large distances might also result from H_2 photodissociation.

The H I emissions show several components with profiles that are quasi-rectangular or Gaussian.

The H I profile of EP Aqr has some common features with that of RS Cnc: a narrow component and a broad Gaussian one centered on the same velocity, which is approximately that obtained from CO rotational lines. These narrow components have CO counterparts, arise in a region close to the central stars and probably trace the present winds (Knapp et al. 1998; Winters et al. 2003). On the other hand, the narrow component in Y CVn has no CO counterpart, arises in a region far from the central star and most probably traces the interaction of the Y CVn outflow with the surrounding ISM.

In general a broad Gaussian-feature should be the evidence of an outflow velocity decreasing with distance to the central star. However another phenomenon which could affect the shape of the H I-profiles is the photo-dissociation of molecular hydrogen. The kinetic energy released in this process corresponds to $\sim$5$-$10 km s^{-1} (Abgrall et al. 2000). Therefore, if some photo-dissociation occurs in a region of the outflow where the hydrogen atoms are not rapidly thermalized, then the 21-cm line-profile will also be affected by this process. High spatial-resolution imaging would be needed to locate the regions where atomic hydrogen is formed.

6. Conclusion

Atomic hydrogen has been detected in emission at 21 cm in the circumstellar environments of EP Aqr and Y CVn for which it appears to be an essential component. The emission is extended and traces H I to large distances, $\sim$1 pc. In the case of Y CVn, our data suggest that we observe also gas at the interface with the ISM. The distribution of H I is not spherically symmetric and the line profiles indicate that the outflow velocity is not constant. The line profiles can be decomposed into separate components that trace different spatial structures. We find velocities shifted by $\sim$1$-$2 km s^{-1}, as compared to those determined from the CO line profiles.

The advent of sensitive interferometers with a large field of view will allow us to map the distribution of atomic hydrogen around sources like EP Aqr and Y CVn. It will provide results on the history of mass loss from red giants which cannot be obtained by other means. We stress the importance of the spectral resolution that should be much better than 1 km s^{-1} to separate the details of the dynamic structures and to compare with the information provided by other tracers like CO.

Acknowledgements. The Nançay Radio Observatory is the Unité scientifique de Nançay of the Observatoire de Paris, associated as Unité de Service et de Recherche (USR) No. B704 to the French Centre National de la Recherche Scientifique (CNRS). The Nançay Observatory also gratefully acknowledges the financial support of the Conseil Régional de la Région Centre in France. This research has made use of the SIMBAD database, operated at CDS, Strasbourg, France and of the NASA's Astrophysics Data System. We are grateful to H. Olofsson for valuable comments. We thank M. Szymczak for a kind exchange of observing time.

References

Abgrall, H., Roueff, E., & Drira, I. 2000, A&AS, 141, 297
Bergeat, J., Knapik, A., & Rutily, B. 2001, A&A, 369, 178
Bowers, P. F., & Knapp, G. R. 1988, ApJ, 332, 299 (BK88)
Dinh-V-Trung, & Nguyen-Q-Rieu 2000, A&A, 361, 601
Dumm, T., & Schild, H. 1998, New Astron., 3, 137
Fleischer, A. J., Gauger, A., & Sedlmayr, E. 1995, A&A, 297, 543
Gérard, E., & Le Bertre, T. 2003, A&A, 397, L17 (Paper II)
Glassgold, A. E., & Huggins, P. J. 1983, MNRAS, 203, 517 (GH83)
González Delgado, D., Olofsson, H., Kerschbaum, F., et al. 2003, A&A, 411, 123
Gussie, G. T., Taylor, A. R., Dewdney, P. E., & Roger, R. S. 1995, MNRAS, 273, 790
Huggins, P. J., Cox, P., Forveille, T., Bachiller, R., & Young, K. 1999, IAU Symp. 191, 425

Izumiura, H., Ukita, N., Kawabe, R., et al. 1987, ApJ, 323, L81
Izumiura, H., Hashimoto, O., Kawara, K., Yamamura, I., & Waters, L. B. F. M. 1996, A&A, 315, L221
Jura, M., Kahane, C., & Omont, A. 1988, A&A, 201, 80
Kahane, C., & Jura, M. 1996, A&A, 310, 952
Kahane, C., Barnbaum, C., Uchida, K., Balm, S. P., & Jura, M. 1998, ApJ, 500, 466
Kerschbaum, F., & Olofsson, H. 1999, A&AS, 138, 299
Knapp, G. R., Young, K., Lee, E., & Jorissen, A. 1998, ApJS, 117, 209
Knapp, G. R., Crosas, M., Young, K., & Ivezić, Ž. 2000, ApJ, 534, 324
Knapp, G. R., Pourbaix, D., Platais, I., & Jorissen, A. 2003, A&A, 403, 993
Lambert, D. L., Gustafsson, B., Eriksson, K., & Hinkle, K. H. 1986, ApJS, 62, 373
Lamers, J. G. L. M., & Cassinelli, J. P. 1999, Introduction to Stellar Winds (Cambridge University Press), 355
Le Bertre, T., & Gérard, E. 2001, A&A, 378, L29 (Paper I)
Maeder, A., & Meynet, G. 1988, A&AS, 76, 411
Neri, R., Kahane, C., Lucas, R., Bujarrabal, V., & Loup, C. 1998, A&AS, 130, 1
Olofsson, H., González Delgado, D., Kerschbaum, F., & Schöier, F. L. 2002, A&A, 391, 1053
Rodríguez, L. F., Goss, W. M., & Williams, R. 2002, ApJ, 574, 179
Schöier, F. L., & Olofsson, H. 2000, A&A, 359, 586
Stephenson, C. B. 1989, A General Catalogue of Cool Galactic Carbon Stars, second edition, Publications of the Warner and Swasey Observatory, 3, No. 2
Taylor, A. R., Gussie, G. T., & Pottasch, S. R. 1990, ApJ, 351, 515
van Driel, W., Pezzani, J., & Gérard, E. 1996, in High Sensitivity Radio Astronomy, ed. N. Jackson, & R. J. Davis (Cambridge Univ. Press), 229
Winters, J. M., Le Bertre, T., Jeong, K. S., Nyman, L.-Å., & Epchtein, N. 2003, A&A, 409, 715
Young, K., Phillips, T. G., & Knapp, G. R. 1993a, ApJS, 86, 517
Young, K., Phillips, T. G., & Knapp, G. R. 1993b, ApJ, 409, 725
Young, K., Cox, P., Huggins, P. J., Forveille, T., & Bachiller, R. 1999, ApJ, 522, 387
Zuckerman, B., Terzian, Y., & Silverglate, P. 1980, ApJ, 241, 1014